Molecular Dynamics of Class A β-lactamases—Effects of Substrate Binding

Olivier Fisette, Stéphane Gagné, and Patrick Lagüe*
Département de Biochimie et de Mcrobiologie, Université Laval and PROTEO and IBIS, Québec (QC), Canada

ABSTRACT The effects of substrate binding on class A β-lactamase dynamics were studied using molecular dynamics simulations of two model enzymes; 40 100-ns trajectories of the free and substrate-bound forms of TEM-1 (with benzylpenicillin) and PSE-4 (with carbenicillin) were recorded (totaling 4.0 μs). Substrates were parameterized with the CHARMM General Force Field. In both enzymes, the Ω loop exhibits a marked flexibility increase upon substrate binding, supporting the hypothesis of substrate gating. However, specific interactions that are formed or broken in the Ω loop upon binding differ between the two enzymes: dynamics are conserved, but not specific interactions. Substrate binding also has a global structuring effect on TEM-1, but not on PSE-4. Changes in TEM-1's normal modes show long-range effects of substrate binding on enzyme dynamics. Hydrogen bonds observed in the active site are mostly preserved upon substrate binding, and new, transient interactions are also formed. Agreement between NMR relaxation parameters and our theoretical results highlights the dynamic duality of class A β-lactamases: enzymes that are highly structured on the ps-ns timescale, with important flexibility on the μs-ms timescale in regions such as the Ω loop.

INTRODUCTION

β-lactam resistance in bacteria is realized through a variety of strategies, the most prevalent of which is the synthesis of the antibiotics-hydrolyzing β-lactamase proteins (reviewed in (1,2)). Class A β-lactamases are an extremely varied group of enzymes that includes extended-spectrum β-lactamases (3). TEM-1 and PSE-4 (Fig. 1) are two model class A β-lactamases and the focus of this work. TEM-1 is a penicillin-cleaving enzyme originating from *Escherichia coli* (4,5), whereas PSE-4 was discovered in opportunistic pathogen *Pseudomonas aeruginosa* (6) and preferentially hydrolyzes carbenicillin (CBC) (Fig. 2 *A*). Class A β-lactamases all share a similar structure made of two domains (one α/β and one all α, see Fig. 1) at the interface of which lies the active site (7–10) (see Fig. 3). Two conserved loops (SDN and Ω) border this site and are involved in catalysis. Five residues, S70, K73, S130, E166, and K243 (R243 in PSE-4) are involved in the two-step acylation-deacylation reaction by which the amide bond in the β-lactam ring of the antibiotics is broken. β-lactam compounds are reviewed in (11,12).

X-ray (8–10,13–17), NMR (18,19), and theoretical (20–34) studies of the catalytic properties of TEM-1 and its variants have shaped our understanding of its serine protease-like reaction mechanism. However, all these studies assume conformations that are near those of x-ray structures. Crystal constraints and protein dynamics are therefore mostly neglected. The first molecular dynamics (MD) simulations of TEM-1 reported no flexibility on the nanosecond timescale (21,22,24) but as trajectory length increased to 5 ns, a motion bringing the E166-bearing Ω loop in contact with the protein core was first observed (23). NMR relaxation studies from our laboratory showed that both TEM-1 and PSE-4 are highly structured on the ps-ns timescale, with slower motions near the active site and in the Ω loop (18,19). Our relaxation NMR studies of PSE-4 are consistent with a flap-like motion in the Ω loop that could promote substrate gating. Complete loop desolvation was observed in another MD study where 10 5-ns trajectories were recorded (30). A more recent MD study from our laboratory characterized TEM-1 dynamics and motions in the Ω loop in more detail, using three 20-ns trajectories (31). However, none of these studies considered the effects of substrate binding, and none compared the dynamics of TEM-1 and PSE-4 except our previous NMR investigation (19). Enzyme dynamics in the bound form could extend our understanding of β-lactamase specificity and catalysis, and help the rational design of novel β-lactam antibiotics (35).

Here, we present results from a simulation study of model β-lactamases TEM-1 and PSE-4 and their preferred substrates, respectively benzylpenicillin (BZP) and CBC that were parameterized to be used with the CHARMM force field. Forty 100-ns MD trajectories were used to compare the bound and free forms of each enzyme, showing that substrate binding affects TEM-1 and PSE-4 in different ways, even though they present 41.5% sequence identity and are highly similar from a structural standpoint (1.3 Å backbone root mean-square deviation (RMSD) between the two enzymes). We highlight the structuring effect of BZP binding on TEM-1, and the increased flexibility of the Ω loop in both enzymes in the bound form. Simulation validation using NMR relaxation order parameters (S^2) shows improved reproduction of protein dynamics compared to

Submitted July 23, 2012, and accepted for publication September 11, 2012.

*Correspondence: patrick.lague@bcm.ulaval.ca

Editor: Patrick Loria.

0006-3495/12/10/1790/12 $2.00

http://dx.doi.org/10.1016/j.bpj.2012.09.009

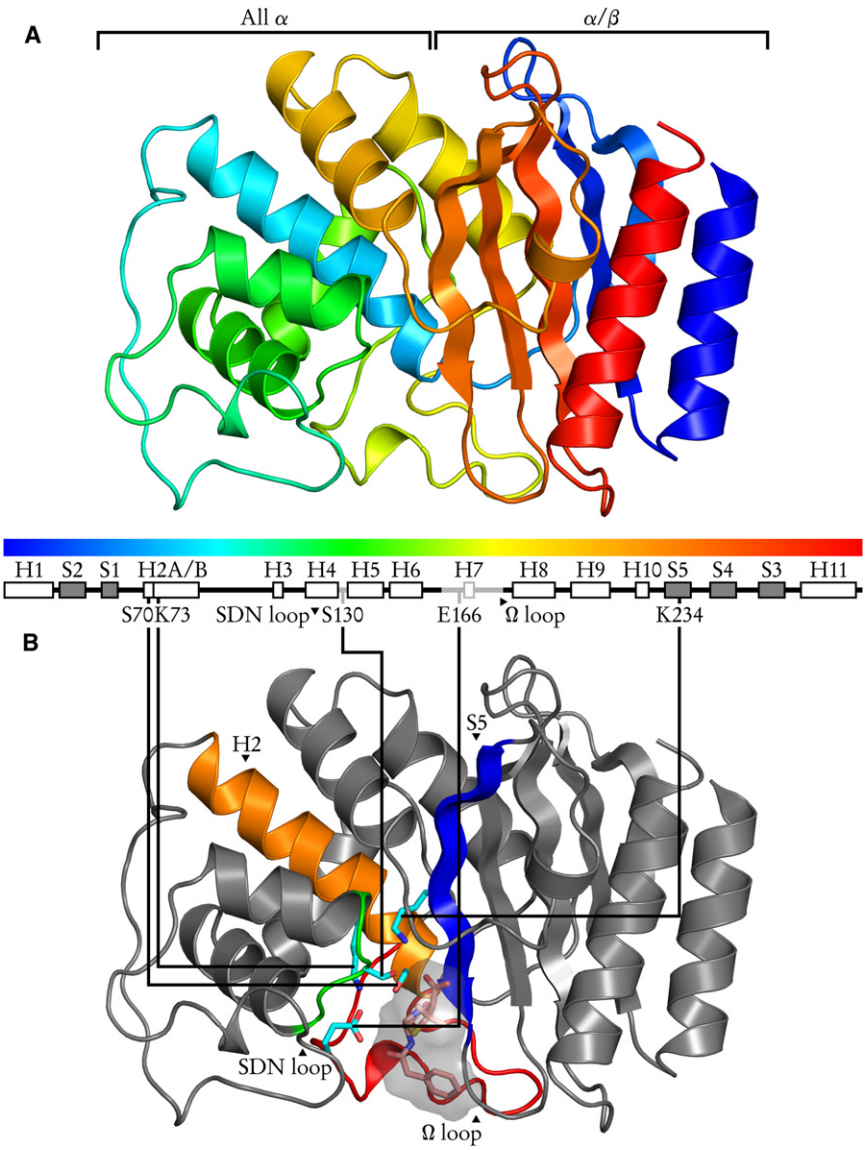

FIGURE 1 General structure of class A β-lactamases, illustrated by the TEM-1/BZP complex. (*A*) The N- and C-terminal sequences form the α/β domain, a five-stranded antiparallel sheet bordered by two helices. The all α domain is a bundle of six helices. (*B*) The active site is at the domain junction. Catalytic residues and substrate are shown as sticks, with CPK-colored atoms: cyan carbons (*pink* for BZP), red oxygens, blue nitrogens, yellow sulphurs. Substrate volumetric surface is shown in translucent gray. Protein elements forming the catalytic site are colored: blue for the S5 strand bearing catalytic K/R234; orange for H2 providing S70 and K73; green for the SDN loop bearing S130; red for the Ω loop with catalytic E166.

previous work (31), and particularly good agreement between experiment and simulation for PSE-4 main chain dynamics. We discuss long-timescale enzyme motions that confirm our hypothesis of dynamical duality (19) in class A β-lactamases: highly structured enzymes on the ps-ns timescale, with flexibility on the μs-ms timescale. We hypothesize that rigidity on the faster timescale allows the precise positioning of the catalytic side chains for catalysis, whereas motions on the slower timescale would facilitate substrate entry and product release, one such motion being the flap of the Ω loop associated with substrate gating.

METHODS

β-lactam parameterization

BZP and CBC (Fig. 2 *A*) were parameterized within the context of CGenFF (CHARMM General Force Field for organic molecules) (36), version 2b5. Because β-lactam antibiotics are mimetic dipeptides, a first attempt was made at parameterizing a minimal β-lactam by analogy with existing amino acid parameters, chiefly proline (due to the disubstituted amide in the lactam cycle). However, molecular mechanics (MM)- and quantum mechanics (QM)-optimized geometries differed significantly (see Fig. S2 in the Supporting Material). We therefore introduced new atom types in CGenFF for the unique chemistry of the β-lactam ring. Subsequent parameter refinement was performed according to the suggested CGenFF protocol and philosophy to obtain transferable parameters that could be used to construct a wide variety of penicillin-like β-lactams.

The sulfur to tertiary carbon bond present in both compounds was not available in CGenFF, and had to be parameterized, using existing parameters and partial charges for carbon-sulfur bonds as reference. The two rings forming the penicillin scaffold were then fused, summing hydrogen charges into neighboring heavy atoms. Finally, benzyl and methyl substituents were added to the scaffold to make the final compounds. A comparison of MM and QM geometries and dipoles is presented in Fig. 2 *B*. All QM calculations were performed with Gaussian 03 (37). Detailed protocol, parameters, and force field files in CHARMM format are given in the Supporting Material.

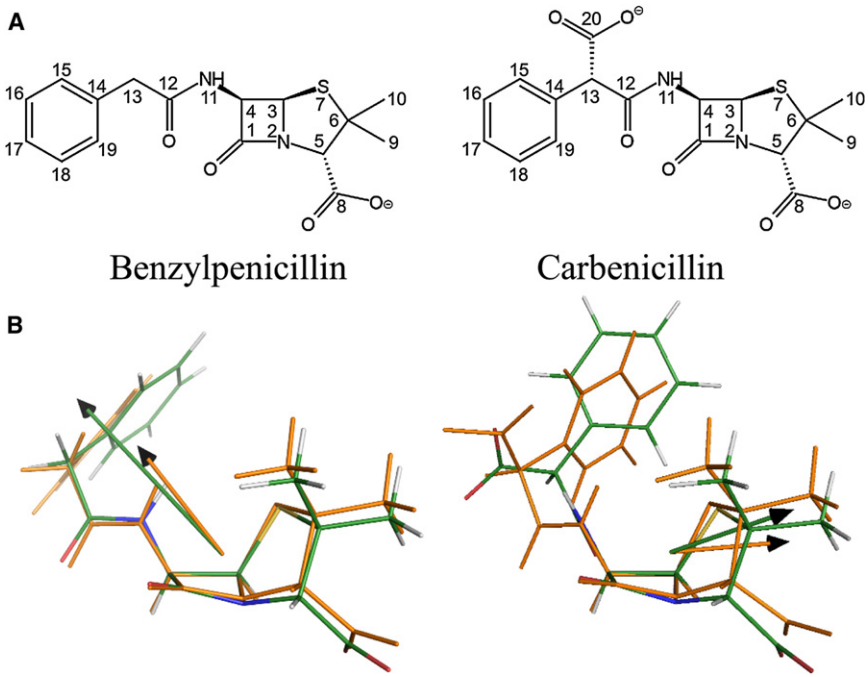

FIGURE 2 (*A*) BZP and CBC structures. The atom numbering used in this work is shown. (*B*) Comparison of BZP and CBC QM- and MM-optimized structures and dipoles after parameterization. QM-optimized structure is in orange. Atoms in MM-optimized structure are CPK-colored: green carbons, red oxygens, blue nitrogens, white hydrogens, yellow sulfurs. Arrows show dipole orientation, in orange and green for QM and MM, respectively.

System generation

The CHARMM (Chemistry at HARvard Molecular Mechanics) program (38), version c35, was used to build all systems. Initial coordinates were taken from crystallographic structures 1XPB (9) and 1G68 (10) for TEM-1 and PSE-4, respectively. Crystallographic waters and ions were removed. Hydrogens were added using CHARMM's *hbuild* function. Initial protonation states were as in previous simulations (31), i.e., all residues have standard protonation states at pH 7.0 except the aspartic acid dyad D214 and D233 that share a proton; D214 was protonated. For PSE-4, five residues are missing from the 1G68 structure: SS at the N-terminus and QSR at the C-terminus. These were added using the internal coordinates method and then relaxed by Langevin dynamics for 5 ns, keeping the rest of the protein fixed.

For the free form, protein was then immersed in a cubic preequilibrated Ewald-compatible TIP3P (39) water box of 78 Å side. Water molecules overlapping with protein (within a distance of 2.8 Å) were removed. Three randomly chosen water molecules were replaced by sodium ions to yield neutral systems of ~47,000 atoms.

The substrate-bound form of both TEM-1 and PSE-4 were generated using the free forms as starting points, before these systems were solvated. Substrate coordinates were taken from crystallographic structure 1FQG (13), which is the BZP acyl-enzyme intermediate in deacylation-defective TEM-1 variant E166N. This 1FQG structure was superposed on the models prepared from 1XPB and 1G68 using RMSD minimization. The resulting substrate coordinates were retained to add the β-lactam to the systems, and the internal coordinates method was used to fill in missing atom positions. The substrate and all atoms within 5 Å of it were then energy minimized for 5000 iterations of the steepest descent algorithm. All other atoms were fixed. Solvation was afterward performed as described for the free enzyme systems.

The resulting active site, for TEM-1 in complex with BZP, is shown in Fig. 3. All catalytic side chains have similar conformations in the crystallographic structure and the computational model; RMSD computed for catalytic residues and substrate (heavy atoms) is 0.15 Å, and there was no steric clash with noncatalytic residues. We used this system generation method, rather than mutating N166 back to E in the 1FQG structure, because such a protocol would have been impossible for PSE-4, for which no acyl-enzyme structure is available. The quality of the resulting TEM-1/BZP system (minimal RMSD to 1FQG and identical side-chain and substrate conformations) argue strongly for the protocol applicability to the similar PSE-4 enzyme. Another substrate-bound PSE-4 computational model Lim2001 (10) suggests an active site conformation that is identical to ours.

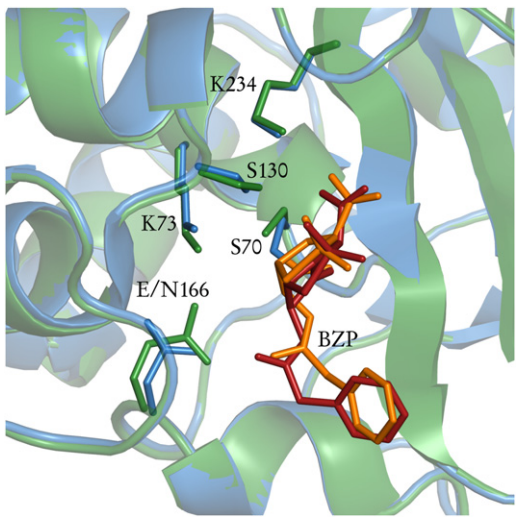

FIGURE 3 TEM-1 active site of the crystallographic structure of E166N mutant (13) and the TEM-1/BZP computational model used in this study. Catalytic side chains and substrate are shown as sticks. Carbons in the crystal structures are green; those in the theoretical model are cyan. BZP in the crystal structure is in orange; BZP theoretical model is in red.

Molecular dynamics

NAMD (Not (just) Another Molecular Dynamics program) (40) was used for all simulations. In the first step, water energy was minimized for 5000 steps while keeping solute fixed. Initial velocities were assigned at

100 K. For each trajectory, a different seed was used when initiating the random number generator, yielding different velocity distributions. Water was relaxed for 1 ns while still keeping the solute fixed. Full system was then relaxed for another ns. Heating to 30°C (303 K) was afterward performed over 1 ns. This temperature was chosen to facilitate comparison with NMR observables recorded at that temperature (18). For each system (TEM-1, PSE-4, TEM-1/BZP, PSE-4/CBC), 10 trajectories were then recorded. The first 10 ns are considered equilibration time, followed by 100 ns production dynamics. Several trajectories were recorded, as opposed to a single longer one, both for feasibility reasons and to avoid known problems with current force fields and very long trajectories (41).

In all simulations, the CHARMM22 force field (42) with CMAP (43) was used. Simulations were performed in the NPT (constant pressure and temperature) ensemble with periodic boundary conditions. The r-RESPA integrator was used with a timestep of 2 fs for electrostatics and 1 fs for all other potentials. Electrostatics was computed by the particle mesh Ewald method, with center of mass drift removal. Van der Waals interactions were smoothed between 10 Å and the cutoff distance of 12 Å using a switching algorithm. Pair lists were computed up to 14 Å and updated at least every 10 timesteps. Langevin damping (1.0 γ coefficient) was used to maintain a constant 30°C temperature. The system was coupled to a Nosé-Hoover Langevin piston to maintain a constant one atmosphere pressure. The length of bonds between hydrogens and heavy atoms were constrained using SETTLE for bonds in water molecules, and SHAKE/RATTLE for all other bonds. No other constraint was applied to the systems, e.g., substrates remained in the active sites only because of protein/substrate interactions. Coordinates were recorded every ps.

Principal component analysis

Principal component analysis (PCA) was performed using the covariance method with the *ptraj* program from the Amber tools (44) package. Only heavy main-chain atoms were considered, and floppy residues were ignored: W at TEM-1 C-terminus; SSK at PSE-4 N-terminus; SQSR at PSE-4 C-terminus. All 10 production trajectories for each system (TEM-1, PSE-4, TEM-1/BZP, and PSE-4/CBC) were used for filling the covariance matrix before diagonalization.

Order parameters

The method used to obtain the S^2 estimates was described in detail and validated in previous work by Fisette et al. (31). Generalized squared order parameters (S^2) for main peptide chain amide (NH) bonds were extracted from their local autocorrelation functions. Global tumbling was removed by a root mean-square minimizing superposition of the C_α of residues involved in α-helix and β-strand secondary structures. By doing so, a fixed reference frame was obtained where only local motions take place. The autocorrelation function $C_I(t)$ is computed for each trajectory (approximating the ensemble using the 100 ns production dynamics) for $t <$ 10 ns, which is the order of magnitude of global tumbling in this system:

$$C_I(t) = \langle P_2[\mu(\tau)\cdot\mu(\tau+t)]\rangle, \quad (1)$$

where P_2 is the second Legendre polynomial: $P_2(x) = (3x^2 - 1)/2$; $\mu(\tau)$ and $\mu(\tau + t)$ are unit vectors describing the chemical bond orientation at times τ and $\tau + t$ in a fixed reference frame. Angle brackets $\langle\ldots\rangle$ denote ensemble averaging. The generalized squared order parameter S^2 is the plateau value of the autocorrelation function:

$$S^2 = \lim_{t\to\infty} C_I(t). \quad (2)$$

See the Supporting Material in (31) for a more detailed analysis. Here, S^2 is estimated as C_I at $t = 10$ ns for each trajectory, and then averaged over the 10 simulations; error is estimated by standard deviation. It should be noted that the time dimension here refers to correlation time, not trajectory time; the full 100 ns of each trajectory is used to compute the autocorrelation function. The choice of $t = 10$ ns (comparable to the protein global tumbling) is necessary to recouple global and local slow dynamics, yielding synthetic S^2 that can be validated against their experimental counterparts; in NMR relaxation, motions slower than the global tumbling cannot be decoupled from the global tumbling itself, and therefore do not contribute to S^2.

RESULTS AND DISCUSSION

Comparison with NMR observables

Generalized squared order parameters (S^2) were computed from the trajectories presented herein and compared to previous NMR relaxation experiments on TEM-1 (18) and PSE-4 (19) and simulations of TEM-1 (31) from our group, as shown in Fig. 4 and Table 1. (Experimental values are available only for the free form.) As expected from the increased conformational space exploration realized with the present simulations, a better agreement between experimental (18) and theoretical results is observed for TEM-1 compared to previous work (31). For PSE-4, an excellent agreement between NMR (19) and simulation results is observed. The most pronounced disagreements are still located in the less ordered regions, and in the Ω loop, where many residues are associated to R_{ex} parameters in NMR studies, suggesting motions on the μs-ms timescale. The only other theoretical study of TEM-1 where S^2 were computed (from 10 5-ns trajectories) (30) exhibited a less precise agreement, although general features were similar: a highly structured enzyme with limited flexibility in the Ω loop on the ps-ns timescale.

Substrate binding affects S^2 of residues in the Ω loop region of both enzymes (Fig. 4, *red circles* versus *blue squares*, and ΔS^2 in panels *B* and *D*, and Table 1), an expected result given our hypothesis of substrate gating and the necessity to position E166 in a catalytically relevant position. Localized differences in S^2 are observed at or nearby other catalytic residues, notably S70, S130, and R234 in PSE-4. Increased R234 flexibility in the bound form is of particular interest, as the catalytic arginine has been shown to be important for the carbenicillinase activity of PSE-4 by relieving a steric clash between S130 side chain and the CBC carboxyl moiety (10). Increased flexibility in the bound form is not seen in TEM-1.

Backbone dynamics

Global RMSD for backbone atoms in all 40 trajectories remain under 2.0 Å at all times, showing simulation stability and the absence of large-scale motions such as partial unfolding (Fig. S9). Average RMSD along sequence is shown for the four different systems (TEM-1, TEM-1/BZP, PSE-4, and PSE-4/CBC) in Fig. 5. Substrate binding affects the two enzymes in different ways. TEM-1 becomes globally more

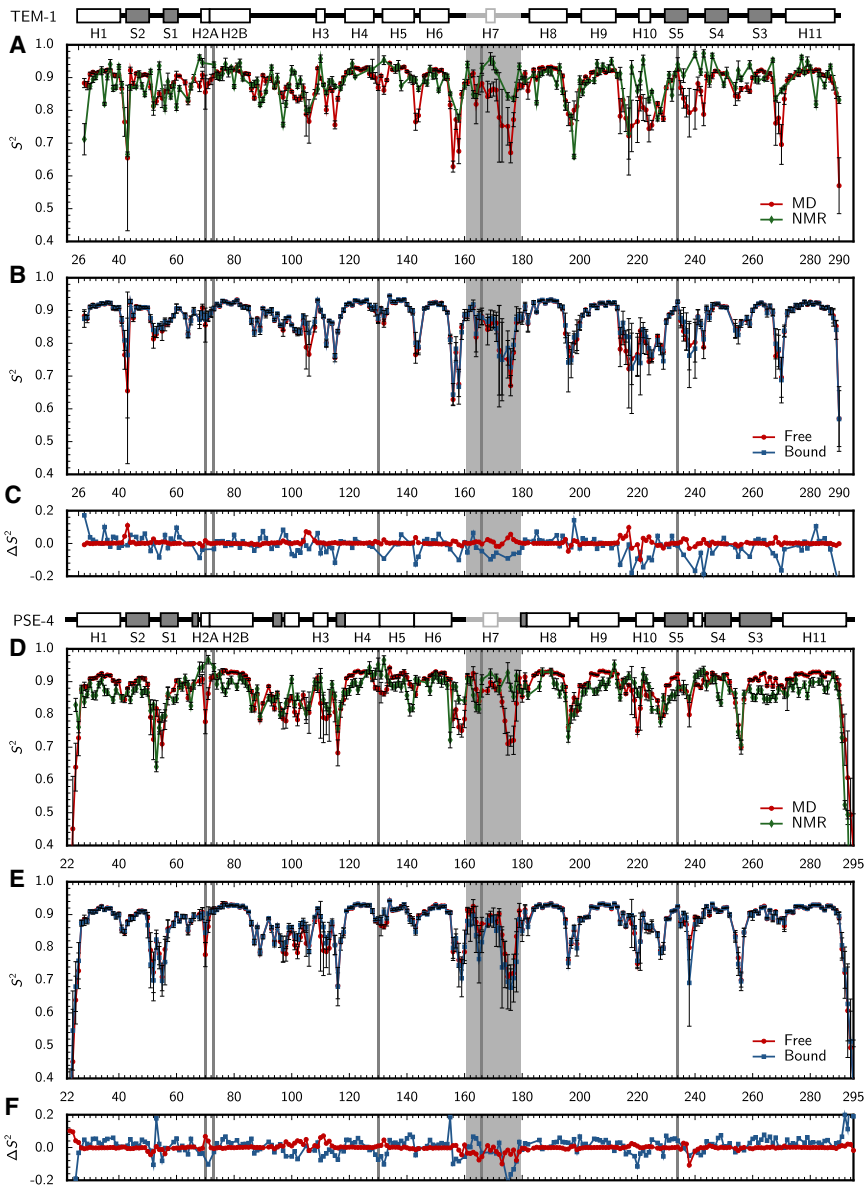

FIGURE 4 Generalized squared order parameters (S^2) along sequence for amide NH bonds in peptide planes. MD-derived (*red circles*) and NMR relaxation (*green diamonds*) S^2 are compared for TEM-1 (*A*) and PSE-4 (*D*). Free (*red circles*) and substrate-bound (*blue squares*) S^2 are compared for TEM-1 (*B*) and PSE-4 (*E*). Difference between MD and NMR S^2 for the free form (*blue squares*), and for the free and bound forms (*red circles*) are given for TEM-1 (*C*) and PSE-4 (*F*). Catalytic residues (S70, K73, S130, E166, and K/R234) are indicated with gray lines, the Ω loop with a light gray box. Indicated above panels are TEM-1 and PSE-4 sequences: α-helices are white boxes; β-strands gray boxes; the Ω loop is in light gray; a vertical bar in H2 indicates the bend between H2A and H2B. NMR data were taken from (18) (TEM-1) and (19) (PSE-4).

rigid (1.02 Å vs. 1.16 Å), except for the C-terminal region of the Ω loop, which becomes more flexible (1.55 Å vs. 1.33 Å for residues 167–179). PSE-4 shows no global change in flexibility (1.04 Å vs. 0.99 Å), but rather an important increase in the motions of the Ω loop and nearby H6-Ω region (1.80 Å vs. 1.05 Å for the Ω loop spanning residues 161–179; 1.18 Å vs. 0.95 Å for the H6-Ω region spanning residues 143–160).

These differences are consistent with those seen for S^2 parameters (Fig. 4). However, the relative amplitude of the changes observed upon substrate binding differ depending on whether RMSD or S^2 are considered. This is particularly the case for the vicinity of the Ω loop, indicating that motions in this region have an important translational component. This is confirmed by observation of PCA normal modes, as discussed in the next paragraph. The translational motions that bring the Ω loop in contact with the protein core are further analyzed in the next section.

Normal modes resulting from PCA analysis of TEM-1 trajectories are shown in Movies S1 and S2. The first five principal components for free form TEM-1 (Movie S1) show the α/β and all α domains rotating and undergoing concerted deformations. The sixth eigenvector shows an independent rocking motion where the Ω loop moves back and forth between solvent and protein core. With the antibiotics in the active site, only the first principal component shows substantial concerted domain rotation/deformation, and motion amplitude is reduced compared to the free form (Movie S2). The second eigenvector in the bound form shows motions essentially limited to the Ω loop. Long-range effects on the dynamics of TEM-1 were also

TABLE 1 Average S^2 from MD and NMR

	TEM-1			PSE-4		TEM-1/BZP	PSE-4/CBC
	MD_1*	MD_2†	NMR‡	MD_2†	NMR§	MD_2†	MD_2†
All residues¶	0.853	0.873	0.886	0.868	0.861	0.876	0.868
α-Helices	0.896	0.907	0.904	0.897	0.881	0.908	0.900
β-Strands	0.876	0.889	0.877	0.878	0.855	0.894	0.877
All loops	0.797	0.829	0.869	0.805	0.824	0.835	0.799
Ω Loop‖	0.748	0.834	0.899	0.849	0.885	0.843	0.813

*Previous simulations from our group (31).
†Present work.
‡NMR relaxation from our group (18) and its reanalysis (31).
§NMR relaxation from our group (19).
¶Except N-terminus and prolines.
‖The Ω loop spans residues 161–179.

observed in other studies (45,46), but caused by the mutation of Y150 (near the active site) rather than by substrate binding. Substrate binding affects TEM-1 dynamics by filling the space at the domain interface, making the concerted domain rotation and deformation observed in the free form more difficult.

The case of PSE-4 is different, as illustrated in Fig. 6, which shows the first PCA normal modes for the free and bound forms of that enzyme, animated in Movies S3 and S4. Substrate binding is correlated to an increase in flexibility in the whole H6-Ω loop region, and a decrease in the H2-H3 interregion. However, there is no global rigidification in PSE-4 as in TEM-1 because the higher flexibility in the region spanning H6 to the C-terminal portion of the Ω loop (inclusively) compensates for the structuring effect of substrate binding at the domain interface. PCA results show that motions in the Ω loop are independent from those in the rest of the structure, and make up most of the observed protein dynamics, driving eigenvectors 1, 3, and 4 in the bound form; concerted domain rotation and deformation appear in later normal modes. By contrast, in the free form, the Ω loop is not involved at all in the first eigenvector. Rather, the most important motions are to be found in the H2-H3 loop. (Motions in the solvent-exposed S1-S2 linker, eigenvector 2, are observed in both the free and bound forms. These will not be discussed because that region is not relevant for catalysis.)

The first, nanosecond-length simulations of TEM-1 (21,22,24) suggested a rigid enzyme with little motion in the vicinity of the Ω loop. This was contradicted shortly afterward by a 5 ns simulation (23), that suggested a rapid motion in the Ω loop, which made contact with the protein core after only 1 ns. Longer simulations (50 ns total) studying desolvation of the Ω loop (30) did not reproduce these results; although an open-close motion was seen in the Ω loop, its timescale was slower than the nanosecond. No significant tethering of the Ω loop to the protein core was observed in 60 ns in a previous work by our group (31), although the Ω loop was shown to be mobile. As the available simulations lengthen and conformational space sampling increases (21,23,30,31), it became apparent that class A β-lactamase residues are highly structured on the ps-ns timescale, but that Ω loop motions happen on the μs-ms timescale, as indicated by the presence of R_{ex} parameters in NMR relaxation. Dynamic duality was first proposed in an NMR study of PSE-4 from our group (19), and is consistent both with the current work and our previous NMR observations of TEM-1 dynamics (18).

It should be noted that equilibrium on the μs-ms timescale cannot be assessed from the current simulations that total 1 μs for each system. Equilibrium on the ps-ns timescale is evident from stable RMSD (see Fig. S9), however, and because the TEM-1/BZP starting structure is similar to that of the acyl-enzyme intermediate, it is unlikely that system equilibration would be responsible for the increased flexibility.

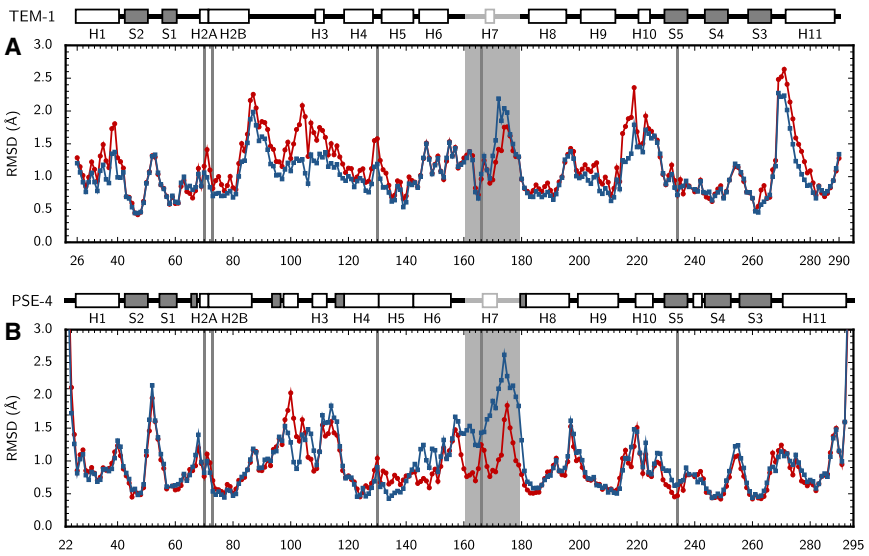

FIGURE 5 RMSD along sequence for the free (*red circles* and *lines*) and substrate-bound (*blue squares* and *lines*) forms of TEM-1 (*A*) and PSE-4 (*B*). Catalytic residues (S70, K73, S130, E166, and K/R234) are indicated with gray lines, the Ω loop with a light gray box. Above panels are TEM-1 and PSE-4 sequences: α-helices are white boxes; β-strands gray boxes; the Ω loop is in light gray; a vertical bar in H2 indicates the bend between H2A and H2B.

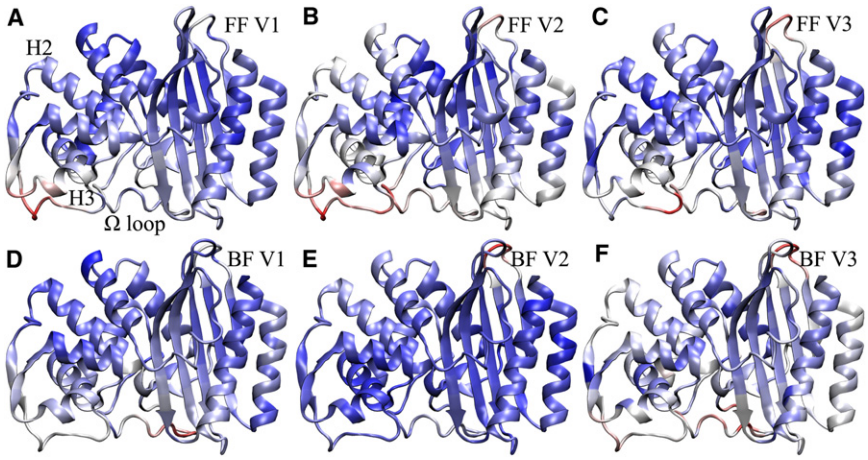

FIGURE 6 Residues involved in the first three PSE-4 normal modes in the free and ligand-bound enzyme. FF: free form; BF: bound form; V: eigenvector number. Residues are colored on a scale from blue to red according to their amplitude of motion within the eigenvector; blue means little amplitude and red high amplitude. The Ω loop and helices H2 and H3 are indicated in the first panel.

Ω loop flexibility

The Ω loop is stabilized by a number of hydrogen bonds and salt bridges established both between residues inside the loop and between residues inside and outside of it. Most of these were first described from crystallographic structures (8,10), whereas others were seen only in simulation studies (23,31). These polar interactions are indexed in Table 2. Fig. 7 presents timeseries of key interactions whose prevalence change in the substrate-bound form for at least one of the two enzymes.

The intra-Ω loop R164 N_{ε}–D179 O_{δ} salt bridge is present in both free TEM-1 (8) and E166Q acyl-enzyme (13) structures. We observe here that substrate binding favors its disruption for TEM-1, but not PSE-4. In free TEM-1, the bridge interconverts between two conformations, where interacting atoms are separated by either 2.5 Å or 3.7 Å. In the bound form, these two conformations are still visited, but larger distances are also observed, where the salt bridge is no longer present. Because these residues are at the extremities of the 161–179 spanning Ω loop, disrupting this salt bridge makes the hinge of the loop more flexible. The homolog interaction in PSE-4 is not affected by substrate binding. It might be that it is not required in PSE-4 due to the aforementioned increased flexibility of the H6-Ω loop region that compensates by making the Ω loop even more flexible in PSE-4 than in TEM-1.

The N/G175 N_H–R65 O_C H-bond has been of particular interest in many dynamics studies of TEM-1. In previous simulations, we did not observe this interaction (31). Here, we observe it in three trajectories, where the Ω loop becomes tethered to the protein core. Two are for the substrate-bound form, one for the free enzyme; the interaction is observed in TEM-1 and PSE-4. Once formed, the H-bond is extremely stable: in two cases, it lasts for the remainder of the trajectory (73 and 34 ns); in the third simulation, the bonds last 16 ns before the loop moves back toward the solvent. Because this is a rare event, the current simulations do not allow a statistically accurate assessment of the timescale of the motion. However, we can rule out the hypotheses of an Ω loop that is either rigid or flexible on the tens of ns timescale. Our current view of the Ω loop, in the light of this work and our previous NMR investigations, is that large-scale motions (loop translation) happen on a timescale exceeding 100 ns (NMR R_{ex} parameters suggest the μs-ms). This is consistent with substrate gating, possibly by a flap-like behavior. These motions are also critical in positioning catalytic E166.

In contrast, some interactions are stabilized by substrate binding. This is the case of R164 N_{η}–E171 O_{ε} in both enzymes, and R178 N_{η}–D176 O_{δ} and R161 N_H–T180 O_C in PSE-4. The increased occupancy of these salt bridges augments the internal rigidity of the Ω loop when the substrate is bound to the β-lactamase. This is consistent with our PCA analysis of the Ω loop presented in the next two paragraphs: upon substrate binding, the Ω loop not only exhibits increased motions, but these motions are more focused, less random.

A precise description of Ω loop motions is difficult from PCA of complete TEM-1 and PSE-4 proteins, because the eigenvectors resulting from this analysis show correlated

TABLE 2 Polar contacts stabilizing the Ω loop

TEM-1*				PSE-4†			
R43	N_{η}	N175	Oδ (31)	No homologous interaction			
R65	N_{η}	N175	O_C‡	R65	N_{η}	G175	O_C‡
R65	N_{η}	N175	O_{δ}	No homologous interaction			
F66	N_H	T181	O_C	F66	N_H	T181	O_C
R161	N_H	T180	O_C	R161	N_H	T180	O_C‡
R161	N_{ε}	H158	O_C	R161	N_{ε}	K158	O_C
R161	N_{ε}	D163	O_{δ}	R161	N_{ε}	D163	O_{δ}
R164	N_{ε}	D179	O_{δ}‡	R164	N_{ε}	D179	O_{δ}
R164	N_{η}	E171	O_{ε}‡	R164	N_{η}	E171	O_{ε}‡
N175	N_H	R65	O_C‡ (23)	G175	N_H	R65	O_C‡ (23)
R178	N_{ε}	D176	O_{δ}	R178	N_{ε}	D176	O_{δ}‡
T181	N_H	F66	O_C	T181	N_H	F66	O_C

*First seen in TEM-1 structure (8) unless noted otherwise.
†First seen in PSE-4 structure (10) unless noted otherwise.
‡Impacted by substrate binding (see main text).

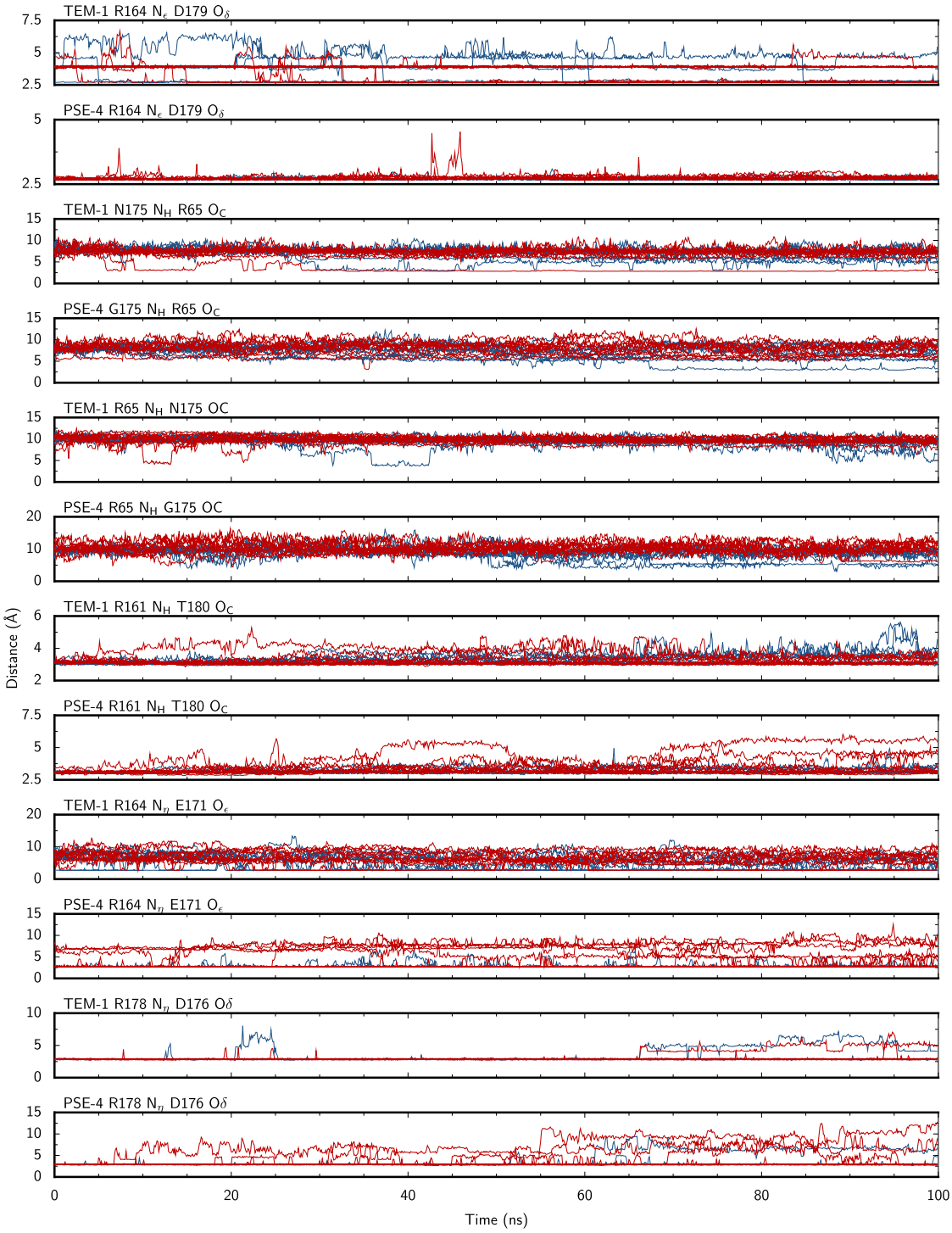

FIGURE 7 Timeseries of key interactions stabilizing the Ω loop in TEM-1 and PSE-4. Each graph shows all 10 simulations of the free enzyme (*red lines*) and the substrate-bound form (*blue lines*). Data points are 10 ps apart and averaged over that time period (10 values).

motions for the whole backbone. A separate PCA focusing only on the Ω loop (residues 161–179) was therefore performed. Normal modes 1 to 3 are shown for both enzymes in Fig. 8. TEM-1 Ω loop first eigenvector shows a sweeping, left-to-right motion (considering a reference frame where the observer faces the Ω loop as in Fig. 1). The second normal mode is an up-and-down motion mainly affecting the C-terminal portion of the loop, and allowing the tethering of the loop to the protein core as described previously. In the third normal mode, the Ω loop moves horizontally; the N-terminal portion is again less affected. PSE-4 shows similar normal modes, but their order of importance is

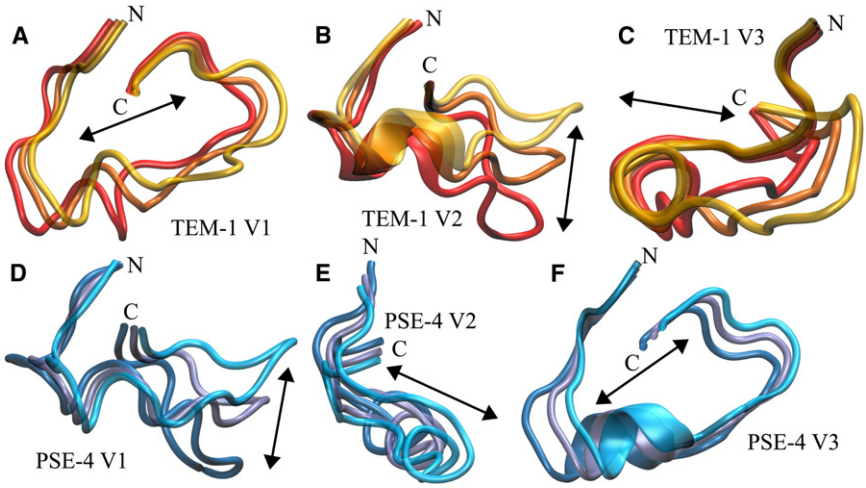

FIGURE 8 Normal modes of the Ω loop (residues 161–179). In each normal mode, the average and extremum structures are shown in different colors. Arrow indicates average direction of motion. *A*, *B*, and *C* are the three first eigenvector for TEM-1 Ω loop. *D*, *E*, and *F* are the three first eigenvectors for PSE-4. In this figure, vectors for enzyme free forms are illustrated; normal modes for bound forms are similar (refer to discussion in main text). The relative amounts of motion represented by the eigenvectors are: TEM-1 free form: 26%, 17%, 12%; TEM-1-bound form: 33%, 28%, 19%; PSE-4 free form: 24%, 14%, 8%; PSE-4 bound form: 39%, 30%, 15%.

different. In PSE-4, the first eigenvector is similar to TEM-1's second. The second vector is similar to TEM-1's first, but with an important difference: the motion also affects the N-terminal portion of the loop. This is consistent with the previously discussed S^2 parameters. PSE-4 third normal mode is identical to the corresponding mode in TEM-1.

Interestingly, normal modes for the bound and free forms are similar, for both TEM-1 and PSE-4. The increase in flexibility observed on substrate binding rather results in the relative importance of the first normal modes. In TEM-1 free enzyme, modes 1 to 3 account for 55% of the Ω loop motions; in the bound form, they represent 80% of motions. A similar tendency is observed in PSE-4, where normal modes 1 to 3 encompass only 47% of all motions in the free form, but 84% in the enzyme-substrate complex. The increase in flexibility shown in S^2, and caused by the destabilization of certain hydrogen bonds in the loop, manifests itself as an increase in the amplitude and relative importance of motions that translate and, to a lesser extent, distort the loop. For both enzymes, eigenvectors 4 and later comprise smaller scale motions. There is more motion in the Ω loop upon substrate binding, but that motion is less random, more focused in the first eigenvectors.

RMSD, S^2, and PCA analysis show that motions in the Ω loop are similar in TEM-1 and PSE-4: the loop is subjected to a translation along three axes, and substrate binding further focuses motions along those axes. This increased loop flexibility is tied to the destabilization of some interactions, and the establishment of new, transient ones. However, Fig. 7 clearly shows that different salt bridges and H-bonds are affected by substrate binding in TEM-1 and PSE-4; protein dynamics are conserved, even though specific interactions are not.

Side-chain dynamics in the active site

β-Lactam substrates BZP and CBC exhibit similar dynamics in the active site of TEM-1 and PSE-4 (respectively). Both molecules are very rigid, with no angle or dihedral angle having an accessible range of $>20^\circ$, with the exception of an unconstrained rotation around the C_{12}–C_{13} bond, present only in BZP/TEM-1 (see Fig. 2 for substrate structure and atom numbering). In PSE-4, this rotation is absent because the CBC-specific carboxyl moeity establishes an intramolecular salt bridge with nearby amide hydrogen H_{11}. This strong interaction makes CBC less flexible than BZP, and brings it away from the Ω loop. This partially explains the difference in Ω loop flexibility between TEM-1 and PSE-4.

In the free enzyme, the active site maintains its high rigidity through a network of hydrogen bonds involving the catalytic residue side chains. This was previously observed in free TEM-1 simulations (31), and sampled exhaustively for both TEM-1 and PSE-4 in this work. Key polar interactions, along with their average occupancy in the trajectories, are indexed in Table 3.

Substrate insertion in the active site allows the formation of new interactions. These are also listed in Table 3 and described here. Fig. 9 shows the active site with bound substrate for both TEM-1 and PSE-4, illustrating these interactions. The amide oxygen in the β-lactam ring (O_1) is stabilized in PSE-4 by transient H-bonding with a catalytic S70 side chain. Interactions with the carboxyl oxygens substituted to the five-membered ring ($O_{8,1/2}$) are key to substrate stabilization. Three catalytic residues in TEM-1, and two in PSE-4, are linked through strong salt bridges to one of these oxygens. In both enzymes, S130 and K/R234 establish salt bridges. S70, on the other hand, only makes contact with the carboxyl in TEM-1, as it is already involved in O_1 stabilization in PSE-4 (discussed previously). These new interactions are consistent with the observed dynamics in the vicinity of active site residues: an increase in S^2 parameters accompanies substrate binding for S70, S130, and K/R234 in both enzymes.

Interestingly, substrate binding does not break the hydrogen bond network observed in the free enzymes. On the contrary, some interactions have increased occupancy

TABLE 3 Key side-chain interactions in the active site

				Occupancy (%)*			
				TEM-1		PSE-4	
Donor		Acceptor		Free	Bound	Free	Bound
S70	O_γ	BZP/CBC	O_1	–	6 (10)	–	50 (22)
S70	O_γ	BZP/CBC	O_8	–	43 (31)	–	3 (6)
S70	O_γ	S130	O_γ	8 (4)	6 (6)	1 (1)	0
S70	O_γ	E166	O_ε	3 (9)	18 (30)	23 (34)	5 (13)
K73	N_ζ	S70	O_γ	69 (30)	63 (39)	55 (27)	86 (16)
K/R234	$N_{\zeta/\eta}$	S70	O_γ	12 (15)	15 (20)	35 (16)	0
K73	N_ζ	S130	O_γ	1 (6)	14 (18)	23 (33)	0
K73	N_ζ	N132	O_δ	55 (30)	86 (14)	47 (37)	87 (21)
K73	N_ζ	E166	O_ε	98 (4)	97 (3)	96 (3)	99 (2)
S130	O_γ	BZP/CBC	O_8	–	63 (27)	–	73 (17)
K/R234	$N_{\zeta/\eta}$	S130	O_γ	84 (18)	51 (33)	77 (33)	Â 98 (21)
N170	N_δ	E166	O_ε	60 (25)	75 (23)	88 (11)	82 (30)
K/R234	$N_{\zeta/\eta}$	BZP/CBC	O_8	–	51 (34)	–	39 (11)
K/R234	$N_{\zeta/\eta}$	S70	O_C	27 (20)	43 (14)	54 (26)	30 (19)
K/R234	$N_{\zeta/\eta}$	I/M127	O_C	38 (25)	10 (15)	35 (14)	48 (10)
K/R234	$N_{\zeta/\eta}$	D/N214	O_δ	23 (17)	8 (10)	93 (13)	90 (5)
K/R234	$N_{\zeta/\eta}$	S235	O_C	38 (25)	82 (14)	13 (9)	69 (19)

Standard deviation between trajectories given in parentheses.
*Given a 3.0 Å cutoff distance.

in the bound forms (see Table 3). This effect is particularly important for K/R234 $N_{\zeta/\eta}$ binding to S235 O_C. Substrate binding therefore has a structuring effect on the active site, as it allows the establishment of new interactions without impacting existing ones. Of particular interest is S70 side-chain dynamics. In PSE-4, the catalytic serine mostly interacts with the carbonyl moeity in the active site, as expected. However, for TEM-1, the side chain can flip, and spends 43% of its time in a position where it interacts with BZP $O_{8,1/2}$ rather than the carbonyl. This conformation may be important for serine activation. Involvement of the carboxyl oxygen (and S130) in S70 deprotonation has been suggested before (20), although it is not the prevalent hypothesis in recent QM/MM studies (25,29).

High standard deviations in Table 3 indicate important variability between trajectories for some interactions. This is an expected result given our hypothesis of dynamic duality in β-lactamases on the μs-ms timescale in and near the active site. Because the current trajectories total 1 μs per system, insufficient statistical sampling on that timescale leads to the observed variability. It can be hypothesized that most of these interactions can be divided into two categories: those associated with small trajectory variability form and break on the ns timescale, while those associated with high standard deviations are involved in motions on the slower, μ-ms timescale.

Some class A β-lactamases (including TEM-1) have been shown to operate at the diffusion limit for their preferred

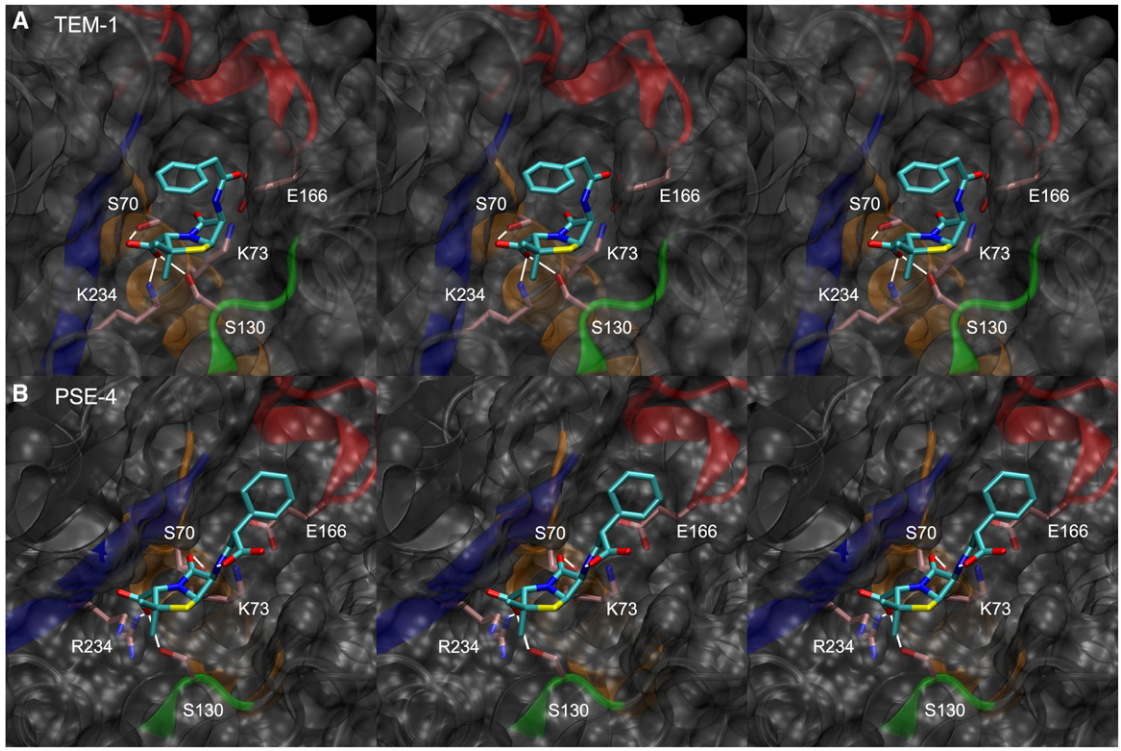

FIGURE 9 Substrate-bound active site for TEM-1/BZP (*A*) and PSE-4/CBC (*B*). Heavy substrate and catalytic side-chain atoms are shown as sticks and CPK-colored, with cyan (*substrate*) or pink (*residues*) carbons. Protein elements forming the catalytic site are colored: blue for S5 strand (K/R234); orange for H2 (S70, K73); green for the SDN loop (S130); red for the Ω loop (E166). H-bonds between catalytic residues and substrate are shown as white lines, as is the intrasubstrate H-bond in CBC. Stereo figure: left pairs are wall-eyed; right pairs cross-eyed.

substrates (47). Dynamic duality may be an important strategy for an enzyme to achieve diffusion-limited speeds. It is a reasonable assumption that the chemistry leading to substrate cleaving makes up only a small part of the catalytic cycle of these β-lactamases; most of the time is spent for substrate diffusion toward the active site, substrate recognition, and product ejection from the active site. With this in mind, rigidity on the ps-ns timescale where chemistry takes place allows a precise, optimal positioning of the catalytic residues. On the other hand, μs-ms motions correspond to the recognition part of the catalytic cycle, accelerating substrate entry and product ejection thanks to the flap-like motion of the Ω loop. Although the present simulations do not allow determining if the Ω loop is involved in both substrate entry and product release, involving gating in both events does seem like an optimal strategy. A certain plasticity in the active site on the μs-ms timescale would favor the recognition of a broad variety of substrates.

CONCLUSION

Using extensive MD simulations, we have shown that substrate binding has long-range effects on the dynamics of class A β-lactamases, and that these effects are different for TEM-1 and PSE-4. TEM-1 becomes globally more rigid, whereas PSE-4 shows increased flexibility in the H6-Ω loop region. In both enzyme-substrate complexes, the Ω loop shows increased translational motions along well-defined axes, and less random motion than in the free form. This reinforces the hypothesis of substrate gating. Because different Ω-loop-stabilizing polar interactions are influenced by substrate binding in TEM-1 and PSE-4, we conclude that the particular dynamical behavior of the Ω loop is possibly a conserved feature of class A β-lactamases, even though specific interactions are not. Stable contacts between the Ω loop and the protein core are shown to happen on the μs-ms timescale, and observed here in only three of the 40 trajectories that total 4.0 μs of simulation. This is consistent with the hypothesis of a dynamical duality in class A β-lactamases: catalysis-related motions on the fast, ps-ns timescale; substrate recognition, and gating motions on the slow, μs-ms timescale. Accelerated MD techniques are a possible venue for characterizing the timescale of these motions and the free energy profile of the Ω loop flap more precisely.

Comparison with NMR observables shows that 1.0 μs of simulation time is adequate to accurately reproduce protein dynamics, except for the Ω loop region. Unfortunately, no NMR S^2 is available in the literature for a substrate-bound class A β-lactamase. This is partially due to experimental difficulties, as it is impossible to saturate diffusion-limited enzymes such as TEM-1 with their preferred substrate for the duration of the relaxation experiments. Nevertheless, NMR measurements with β-lactamase inhibitor-complexed enzymes would further our understanding of these enzyme's dynamics. With simulations now routinely exceeding 100 ns, and the possibility of using accelerated MD techniques for further exploring the role of the Ω loop, residual dipolar coupling order parameters or relaxation dispersion experiments, in particular, would provide additional insights into μs-ms dynamics, with the caveat that using inhibitors may influence dynamics differently than the conventional substrate.

The differing behavior of the catalytic serine in TEM-1 and PSE-4 shows that active site dynamics vary between the penicillin- and CBC-cleaving enzymes. The important conformational space sampling achieved here provides interesting starting points for QM/MM studies that would take into account important dynamic events, such as Ω loop position. Finally, parameterization of the penicillin scaffold makes a variety of antibiotics amenable to simulation, facilitating the study of substrate specificity in class A β-lactamases.

SUPPORTING MATERIAL

Detailed protocol, parameters, and force field files in CHARMM format for the parameterization of β-lactam antibiotics; global main-chain RMSD and correlation functions figures supporting the backbone dynamics results section; essential dynamics movies, and movie list are available at http://www.biophysj.org/biophysj/supplemental/S0006-3495(12)01021-1.

This work was supported by grants from the Natural Sciences and Engineering Research Council of Canada (NSERC), the Fonds de recherche du Québec – Nature et technologies (FRQ_NT), and the Canadian Foundation for Innovation (CFI). We thank Compute Canada and CLUMEQ for the provision of computer time on the Colosse supercomputer.

REFERENCES

1. Hall, B. G., and M. Barlow. 2004. Evolution of the serine β-lactamases: past, present and future. *Drug Resist. Updat.* 7:111–123.

2. Fisher, J. F., S. O. Meroueh, and S. Mobashery. 2005. Bacterial resistance to β-lactam antibiotics: compelling opportunism, compelling opportunity. *Chem. Rev.* 105:395–424.

3. Bush, K., and G. A. Jacoby. 2010. Updated functional classification of β-lactamases. *Antimicrob. Agents Chemother.* 54:969–976.

4. Datta, N., and P. Kontomichalou. 1965. Penicillinase synthesis controlled by infectious R factors in Enterobacteriaceae. *Nature.* 208:239–241.

5. Salverda, M. L. M., J. A. De Visser, and M. Barlow. 2010. Natural evolution of TEM-1 β-lactamase: experimental reconstruction and clinical relevance. *FEMS Microbiol. Rev.* 34:1015–1036.

6. Furth, A. J. 1975. Purification and properties of a constitutive β-lactamase from *Pseudomonas aeruginosa* strain Dalgleish. *Biochim. Biophys. Acta.* 377:431–443.

7. Dideberg, O., P. Charlier, …, J. M. Ghuysen. 1987. The crystal structure of the β-lactamase of *Streptomyces albus* G at 0.3 nm resolution. *Biochem. J.* 245:911–913.

8. Jelsch, C., L. Mourey, …, J. P. Samama. 1993. Crystal structure of *Escherichia coli* TEM1 β-lactamase at 1.8 A resolution. *Proteins.* 16:364–383.

9. Fonzé, E., P. Charlier, …, J. M. Frère. 1995. TEM1 beta-lactamase structure solved by molecular replacement and refined structure of the S235A mutant. *Acta Crystallogr. D Biol. Crystallogr.* 51:682–694.
10. Lim, D., F. Sanschagrin, …, N. C. Strynadka. 2001. Insights into the molecular basis for the carbenicillinase activity of PSE-4 beta-lactamase from crystallographic and kinetic studies. *Biochemistry.* 40:395–402.
11. Singh, G. S. 2004a. β-lactams in the new millennium. Part-I: monobactams and carbapenems. *Mini Rev. Med. Chem.* 4:69–92.
12. Singh, G. S. 2004b. β-lactams in the new millennium. Part-II: cephems, oxacephems, penams and sulbactam. *Mini Rev. Med. Chem.* 4:93–109.
13. Strynadka, N. C., H. Adachi, …, M. N. James. 1992. Molecular structure of the acyl-enzyme intermediate in beta-lactam hydrolysis at 1.7 A resolution. *Nature.* 359:700–705.
14. Minasov, G., X. Wang, and B. K. Shoichet. 2002. An ultrahigh resolution structure of TEM-1 beta-lactamase suggests a role for Glu166 as the general base in acylation. *J. Am. Chem. Soc.* 124:5333–5340.
15. Wang, X., G. Minasov, …, B. K. Shoichet. 2003. Recognition and resistance in TEM beta-lactamase. *Biochemistry.* 42:8434–8444.
16. Wang, J., T. Palzkill, and D.-C. Chow. 2009. Structural insight into the kinetics and DeltaCp of interactions between TEM-1 beta-lactamase and beta-lactamase inhibitory protein (BLIP). *J. Biol. Chem.* 284:595–609.
17. Docquier, J. D., M. Benvenuti, …, S. Mangani. 2011. Structure of the extended-spectrum β-lactamase TEM-72 inhibited by citrate. *Acta Crystallogr. Sect. F Struct. Biol. Cryst. Commun.* 67:303–306.
18. Savard, P.-Y., and S. M. Gagné. 2006. Backbone dynamics of TEM-1 determined by NMR: evidence for a highly ordered protein. *Biochemistry.* 45:11414–11424.
19. Morin, S., and S. M. Gagné. 2009. NMR dynamics of PSE-4 beta-lactamase: an interplay of ps-ns order and mus-ms motions in the active site. *Biophys. J.* 96:4681–4691.
20. Díaz, N., D. Suárez, …, K. M. Merz. 2001. Acylation of class A β-lactamases by penicillins: a theoretical examination of the role of serine 130 and the β-lactam carboxylate group. *J. Phys. Chem. B.* 105:11302–11313.
21. Díaz, N., T. L. Sordo, …, D. Suárez. 2003. Insights into the acylation mechanism of class A beta-lactamases from molecular dynamics simulations of the TEM-1 enzyme complexed with benzylpenicillin. *J. Am. Chem. Soc.* 125:672–684.
22. Díaz, N., D. Suárez, …, T. L. Sordo. 2005. Molecular dynamics simulations of the TEM-1 beta-lactamase complexed with cephalothin. *J. Med. Chem.* 48:780–791.
23. Roccatano, D., G. Sbardella, …, F. Mazza. 2005. Dynamical aspects of TEM-1 beta-lactamase probed by molecular dynamics. *J. Comput. Aided Mol. Des.* 19:329–340.
24. Meroueh, S. O., P. Roblin, …, S. Mobashery. 2002. Molecular dynamics at the root of expansion of function in the M69L inhibitor-resistant TEM beta-lactamase from *Escherichia coli*. *J. Am. Chem. Soc.* 124:9422–9430.
25. Meroueh, S. O., J. F. Fisher, …, S. Mobashery. 2005. Ab initio QM/MM study of class A beta-lactamase acylation: dual participation of Glu166 and Lys73 in a concerted base promotion of Ser70. *J. Am. Chem. Soc.* 127:15397–15407.
26. Hermann, J. C., L. Ridder, …, H. D. Höltje. 2003. Identification of Glu166 as the general base in the acylation reaction of class A beta-lactamases through QM/MM modeling. *J. Am. Chem. Soc.* 125: 9590–9591.
27. Hermann, J. C., C. Hensen, …, H. D. Höltje. 2005. Mechanisms of antibiotic resistance: QM/MM modeling of the acylation reaction of a class A beta-lactamase with benzylpenicillin. *J. Am. Chem. Soc.* 127:4454–4465.
28. Hermann, J. C., L. Ridder, …, A. J. Mulholland. 2006. Molecular mechanisms of antibiotic resistance: QM/MM modelling of deacylation in a class A beta-lactamase. *Org. Biomol. Chem.* 4:206–210.
29. Hermann, J. C., J. Pradon, …, A. J. Mulholland. 2009. High level QM/MM modeling of the formation of the tetrahedral intermediate in the acylation of wild type and K73A mutant TEM-1 class A beta-lactamase. *J. Phys. Chem. A.* 113:11984–11994.
30. Bös, F., and J. Pleiss. 2009. Multiple molecular dynamics simulations of TEM β-lactamase: dynamics and water binding of the ω-loop. *Biophys. J.* 97:2550–2558.
31. Fisette, O., S. Morin, …, S. M. Gagné. 2010. TEM-1 backbone dynamics-insights from combined molecular dynamics and nuclear magnetic resonance. *Biophys. J.* 98:637–645.
32. Lamotte-Brasseur, J., G. Dive, …, J. M. Ghuysen. 1991. Mechanism of acyl transfer by the class A serine beta-lactamase of *Streptomyces albus* G. *Biochem. J.* 279:213–221.
33. Golemi-Kotra, D., S. O. Meroueh, …, S. Mobashery. 2004. The importance of a critical protonation state and the fate of the catalytic steps in class A beta-lactamases and penicillin-binding proteins. *J. Biol. Chem.* 279:34665–34673.
34. Massova, I., and P. A. Kollman. 2002. pKa, MM, and QM studies of mechanisms of beta-lactamases and penicillin-binding proteins: acylation step. *J. Comput. Chem.* 23:1559–1576.
35. Chaudhuri, R., O. Carrillo, …, M. Orozco. 2012. Application of drug-perturbed essential dynamics/molecular dynamics (ED/MD) to virtual screening and rational drug design. *J. Chem. Theory Comput.* 8:2204–2214.
36. Vanommeslaeghe, K., E. Hatcher, …, A. D. Mackerell, Jr. 2010. CHARMM general force field: a force field for drug-like molecules compatible with the CHARMM all-atom additive biological force fields. *J. Comput. Chem.* 31:671–690.
37. Frisch, M. J., G. W. Trucks, …, M. Challacombe, P.M. 2003. Gaussian 03. Gaussian, Wallingford, CT.
38. Brooks, B. R., C. L. Brooks, 3rd, …, M. Karplus. 2009. CHARMM: the biomolecular simulation program. *J. Comput. Chem.* 30:1545–1614.
39. Price, D. J., and C. L. Brooks, 3rd. 2004. A modified TIP3P water potential for simulation with Ewald summation. *J. Chem. Phys.* 121:10096–10103.
40. Phillips, J. C., R. Braun, …, K. Schulten. 2005. Scalable molecular dynamics with NAMD. *J. Comput. Chem.* 26:1781–1802.
41. Lange, O. F., D. van der Spoel, and B. L. de Groot. 2010. Scrutinizing molecular mechanics force fields on the submicrosecond timescale with NMR data. *Biophys. J.* 99:647–655.
42. MacKerell, Jr., A. D., M. Bashford, …, M. Karplus. 1998. All-atom empirical potential for molecular modeling and dynamics studies of proteins. *J. Phys. Chem. B.* 102:3586–3616.
43. Mackerell, Jr., A. D., M. Feig, and C. L. Brooks, 3rd. 2004. Extending the treatment of backbone energetics in protein force fields: limitations of gas-phase quantum mechanics in reproducing protein conformational distributions in molecular dynamics simulations. *J. Comput. Chem.* 25:1400–1415.
44. Case, D. A., T. E. Cheatham, 3rd, …, R. J. Woods. 2005. The Amber biomolecular simulation programs. *J. Comput. Chem.* 26:1668–1688.
45. Doucet, N., P.-Y. Savard, …, S. M. Gagné. 2007. NMR investigation of Tyr105 mutants in TEM-1 beta-lactamase: dynamics are correlated with function. *J. Biol. Chem.* 282:21448–21459.
46. Doucet, N., and J. N. Pelletier. 2007. Simulated annealing exploration of an active-site tyrosine in TEM-1 beta-lactamase suggests the existence of alternate conformations. *Proteins.* 69:340–348.
47. Hardy, L. W., and J. F. Kirsch. 1984. Diffusion-limited component of reactions catalyzed by *Bacillus cereus* beta-lactamase I. *Biochemistry.* 23:1275–1282.